Supplement of Earth Syst. Sci. Data, 18, 7981–8002, 2026
https://doi.org/10.5194/essd-18-7981-2026-supplement
© Author(s) 2026. CC BY 4.0 License.



Open Access Earth System Science Data

Supplement of

The Standardized Soil Moisture-Temperature Compound Index (SSTCI): daily scale global data set and event catalogue for compound dry-hot extremes (1961–2023)

Rukhshinda Aftab et al.

Correspondence to: Guojie Wang (gwang_nuist@163.com)

The copyright of individual parts of the supplement might differ from the article licence.

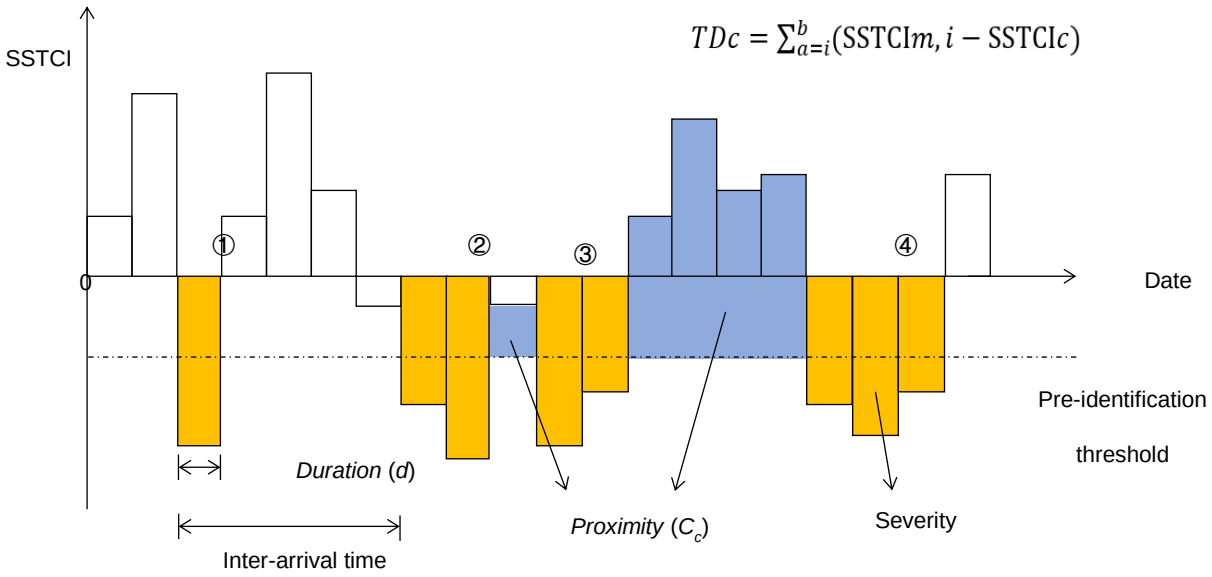


Figure S1: Conceptual illustration of the identification of CDHEs

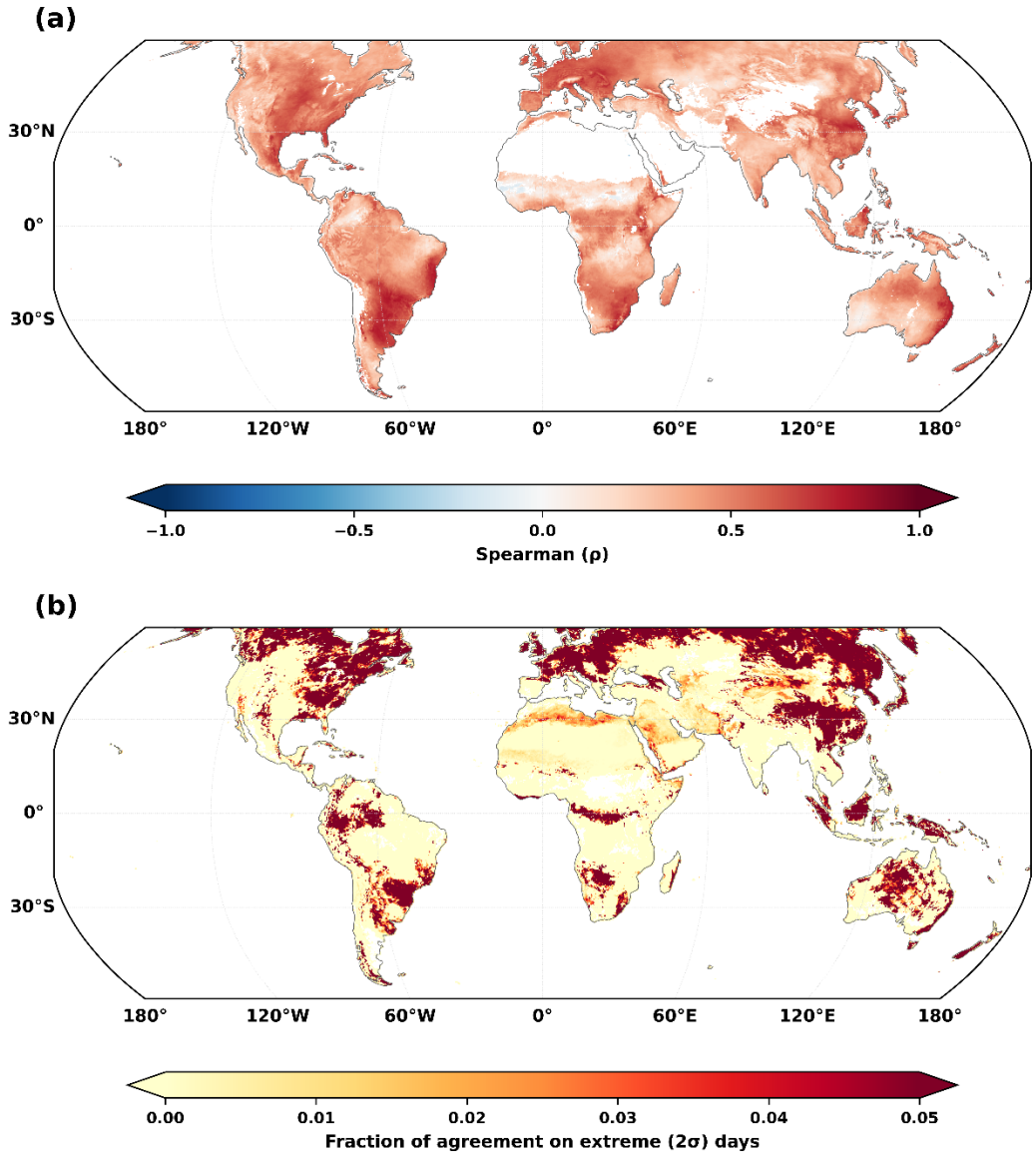


Figure S2. Agreement between the Standardized Antecedent Soil Moisture Index (SASMI) and the Standardized Precipitation–Evapotranspiration Index (SPEI), computed at daily resolution over 2001–2020. (a) Spearman rank correlation; only statistically significant values ($\alpha = 0.05$) are shown, and non-significant pixels are masked. Warm colours indicate positive correlation and cool colours indicate negative correlation. (b) Per-pixel fraction of agreement on extreme (2σ) days, calculated as the number of days both indices fall below -2 divided by the number of days either index falls below -2. Warmer colours indicate higher agreement on the timing of extreme dry days. Barren and low-variability regions masked in the SPEI product appear as no data in both panels.

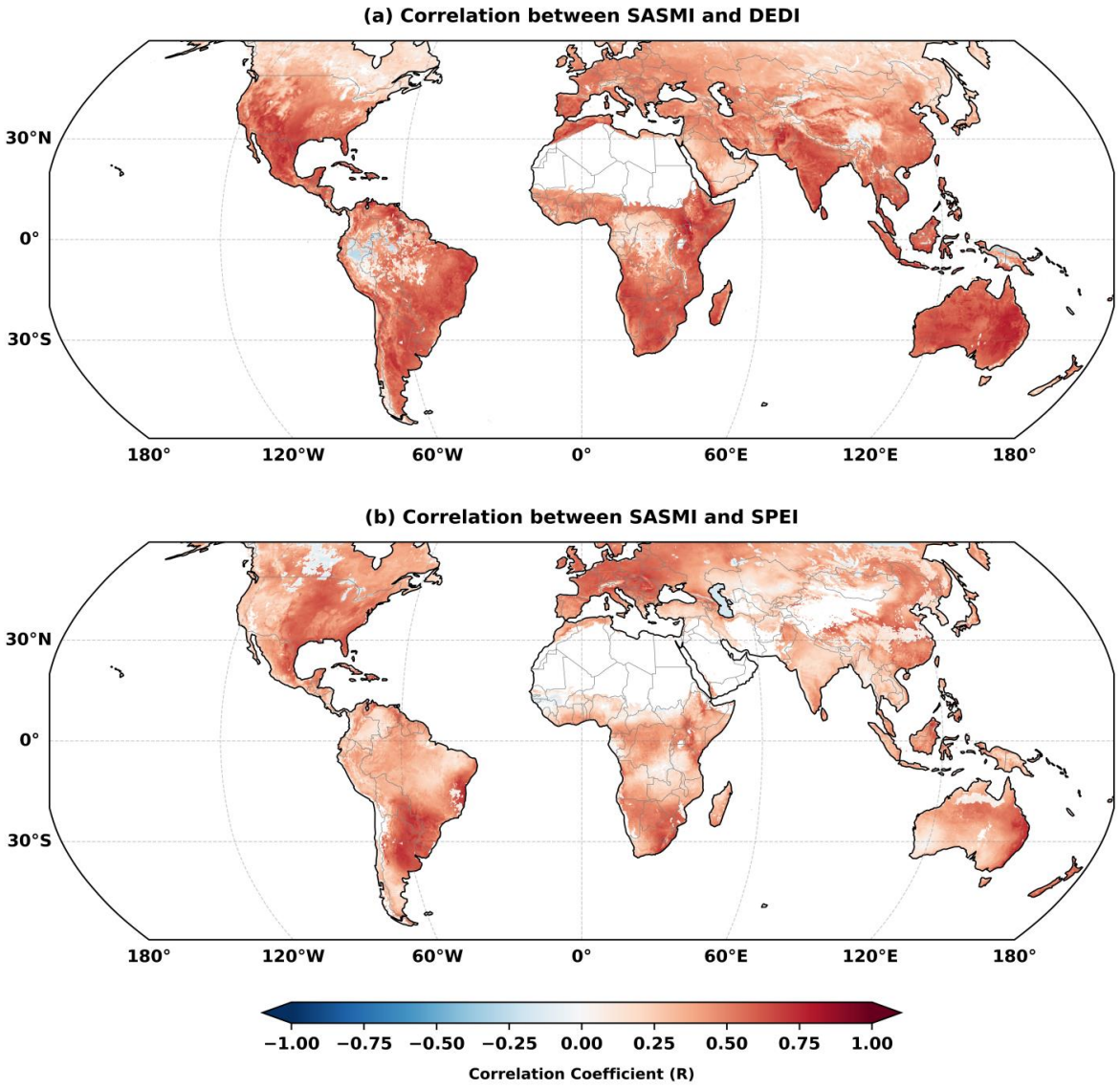


Figure S3. Spatial Pearson correlation between the Standardized Antecedent Soil Moisture Index (SASMI) and two established daily drought indicators: (a) the Daily Evapotranspiration Deficit Index (DEDI) and (b) the Standardized Precipitation–Evapotranspiration Index (SPEI). Correlations are calculated at daily resolution over the common analysis period, and only statistically significant correlations ($\alpha = 0.05$) are shown; non-significant pixels are masked. Warm colors indicate positive correlation and cool colors indicate negative correlation between the indices.

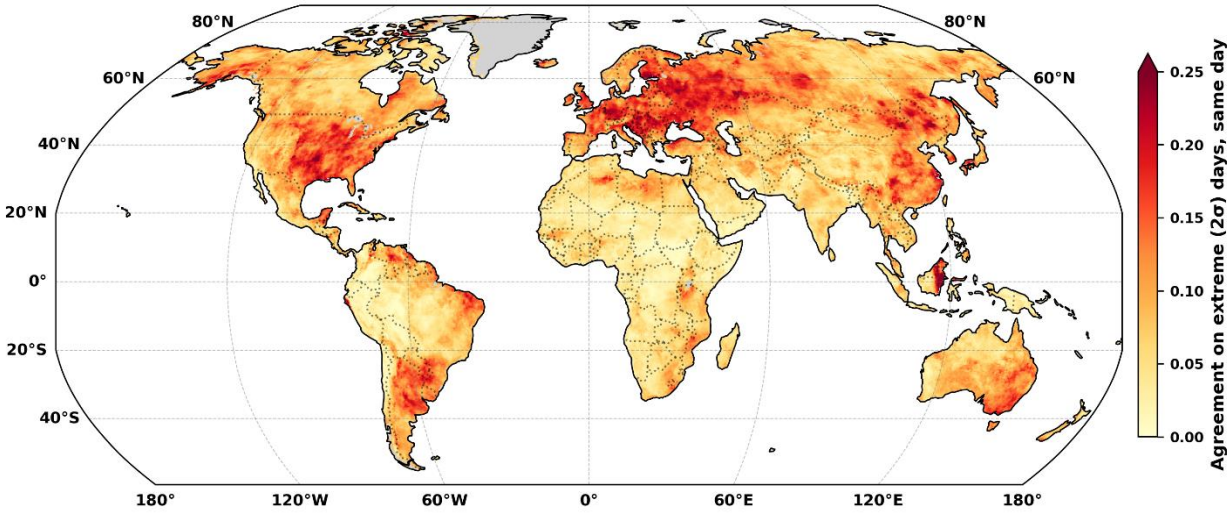


Figure S4. Per-pixel fraction of agreement between SSTCI and the Standardized Compound Dry–Hot Index (SCDHI) on extreme (2σ) days over 1981–2013, requiring exact same-day co-occurrence. Agreement is calculated as the number of days both indices fall below −2 divided by the number of days either index does. The corresponding map allowing a ±5-day tolerance is shown in Fig. 3b

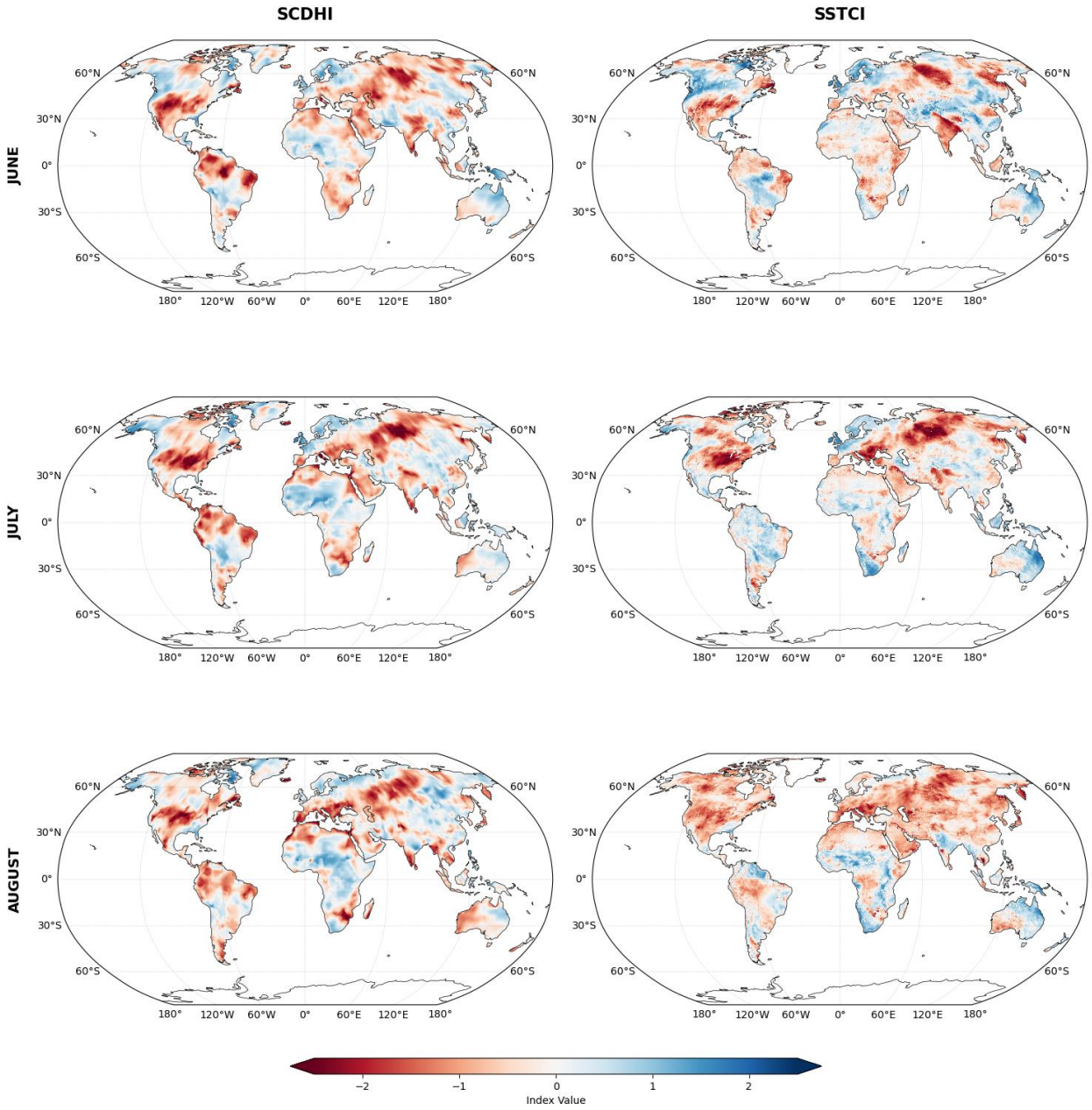


Figure S5: Spatial pattern comparison of standardized compound dry hot index(SCDHI) and standardized soil moisture temperature index (SSTCI) for summer 2012.

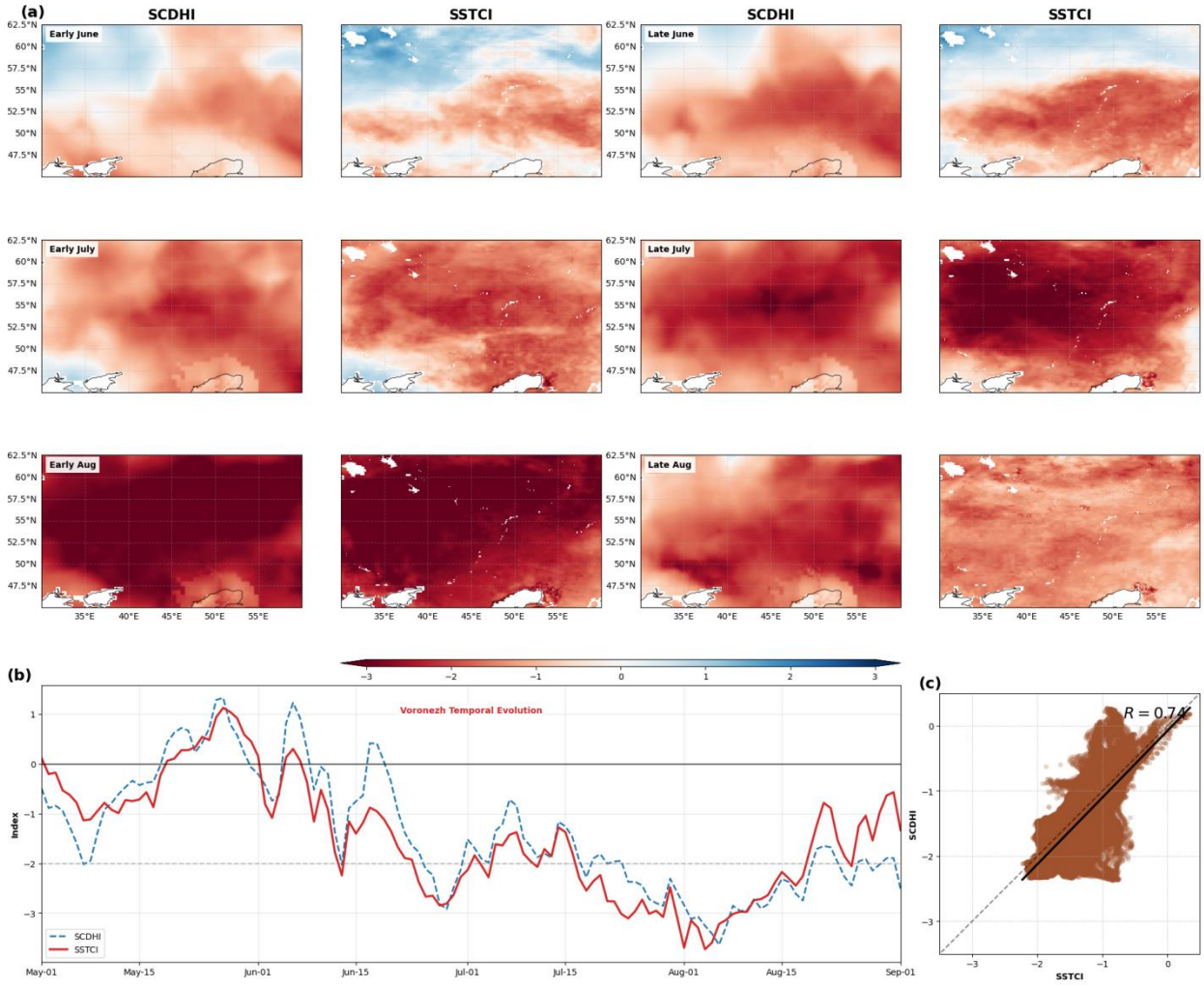


Figure S6: Spatiotemporal analysis of the 2010 Western Russia CDHE event. (a) 15-day mean evolution of SCDHI and SSTCI (June–August) (b) Daily time series for Voronezh (May–September) showing tight coupling between SSTCI and SCDHI (c) JJA spatial correlation across the Western Russia domain (45-65N^{o},30-60E^{0})). The robust positive relationship (R = 0.74) confirms the indices' agreement during extreme conditions.

CWT analysis of SSTCI on selected Basins

To investigate the changes in the timescales of increases in event persistence and occurrence (Fig. 3-4), we applied Continuous Wavelet Transform (CWT) analysis to the daily SSTCI time series (negative values of SSTCI only used to show dry-hot conditions). Here, we selected the Yangtze River Basin (YRB) and the Amazon Basin as representative case studies for this analysis, as they represent distinct hydro-climatic regimes. The former is a subtropical monsoon system and the latter, a tropical rainforest, where both exhibited some of the strongest positive duration trends in our global analysis. Figure 8 illustrates the results for the Yangtze River Basin (panel a) and the Amazon Basin (panel b) over the 1961–2023 period. The upper subpanels display the standardized daily SSTCI time series, while the lower subpanels present the continuous wavelet power spectrum with periods (in days) on the y-axis, highlighting variability across sub-monthly (~10–30 days), seasonal (~40–400 days), and multi-year (>~500 days) scales.

In the YRB (Fig. 8a), sub-monthly signals are evident throughout the record. However, the seasonal band exhibits a distinct regime shift; while sporadic before 2000, it becomes intensified and nearly continuous from ~2003 onward (centered at ~200–350 days). Since 2000, broad interannual power (>~500 days) has emerged more frequently, forming vertical columns of coherence that connect seasonal patterns to multi-year scales. These cross-scale episodes are most pronounced during 2004–2011 and 2015–2023. Similarly, the Amazon Basin (Fig. 8b) shows persistent sub-monthly variability, but with a marked broadening and intensification of the seasonal band after ~2005. From the mid-2000s onward, the spectrum reveals large, contiguous zones of multi-year power that repeatedly bridge upward from the seasonal band, indicating strong cross-scale coupling. This organization is particularly robust during the mid-2000s and the 2015–2023 period. Collectively, both basins exhibit a late record shift toward enhanced seasonal to interannual organization and stronger cross-scale connectivity. The YRB is characterized by an earlier emergence of a focused, continuous seasonal band, whereas the Amazon displays broader seasonal power with more extensive vertical integration into multi-year timescales.

Collectively, the continuous wavelet analysis reveals a synchronized regime shift in both basins, characterized by the post-2000 emergence of vertical spectral bridges that link seasonal variability to interannual timescales. This spectral coalescence provides a physical explanation for the lengthening trends in Fig.7: CDHEs are transitioning from stochastic, short-lived pulses to sustained, resonant regimes. This finding highlights the necessity of the SSTCI's daily resolution, which is required to resolve these critical cross-scale interactions that coarser monthly indices would miss.

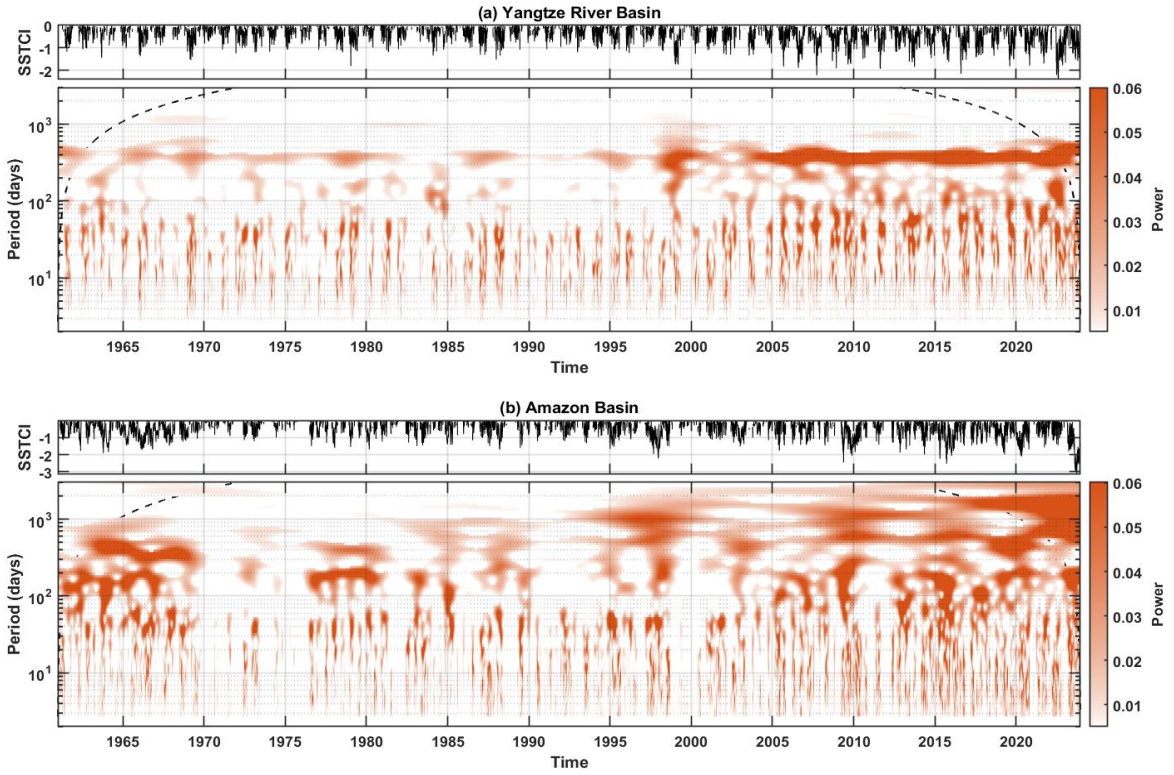


Figure S7. Daily SSTCI variability and continuous wavelet power spectra for two hydro-climatically distinct hotspot basins: (a) the Yangtze River Basin and (b) the Amazon Basin, over 1961–2023. In each panel, the upper subpanel shows the standardized daily SSTCI time series, while the lower subpanel shows the continuous wavelet power spectrum with period (days) on the vertical axis, resolving variability across different scales.

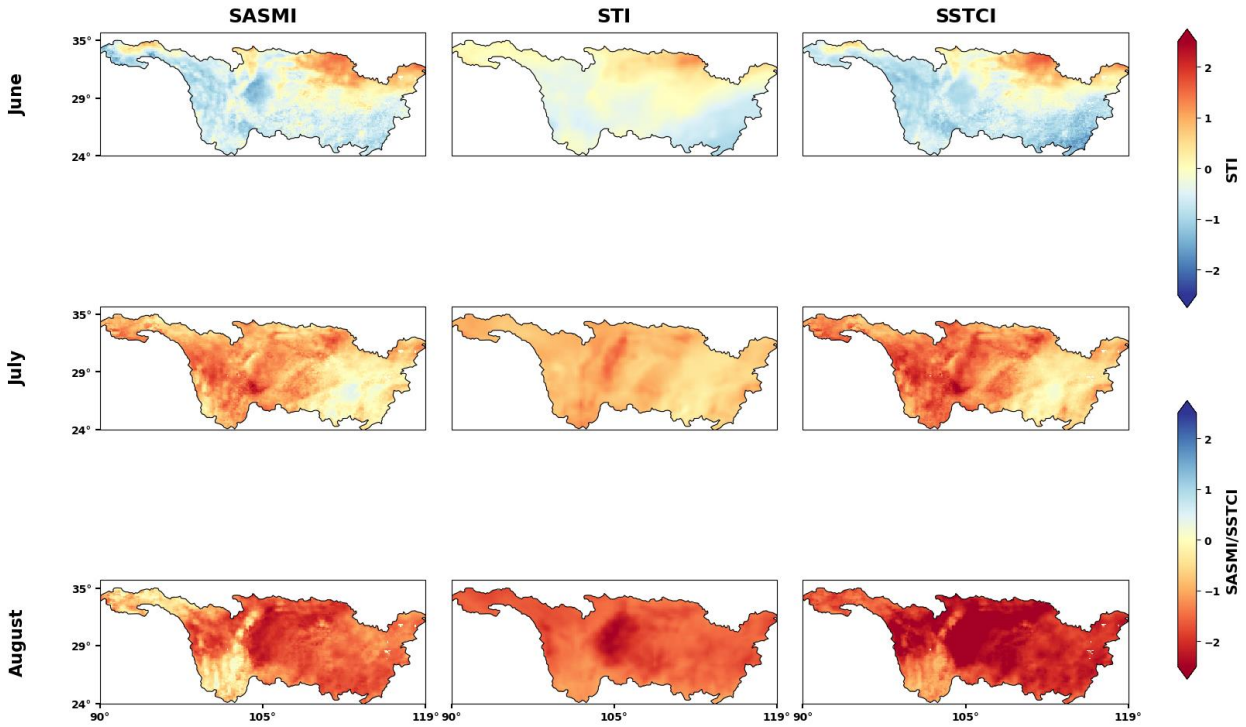


Figure S8: Monthly Evolution of the CDHE 2022 event over the Yangtze River basin

Table S1: Categories of compound dry and hot conditions thresholds based on SSTCI

Category	**SSTCI Threshold**
Abnormal	−-0.80, −0.50
Light	−1.30, −0.80
Moderate	−1.60, −1.30
Heavy	−2.0, −1.60
Extreme	**≤ −2**

Table S2: Selected latitude and longitude range for the Global Radar plots

Region	Years	Lon Min	Lon Max	Lat Min	Lat Max
Northern Italy (Po Basin)	2022	7.5°E	13.2°E	44.4°N	46.4°N
Southwest US (Mogollon Rim)	2021	112.3°W	108.9°W	33.5°N	35.8°N
Pantanal (Brazil)	2020	58.5°W	55.0°W	20.5°S	16.5°S
South Africa (central–northern interior)	2015–2016	20.0°E	30.5°E	28.5°S	22.0°S
Northeast Australia	2019	142.0°E	151.0°E	22.0°S	12.0°S
Yangtze River Basin (YRB)	2022	103.0°E	123.0°E	25.0°N	35.0°N

Table S3. Summary of historical CDHE events identified for an example pixel (**28.9°N, 108.9°E)**

Number	Duration	Total severity	Intensity	Start Year	Start Month	Start Day	End Year	End Month	End Day
1	17	41.87	2.46	1963	2	19	1963	3	7
2	6	13.91	2.32	1965	5	28	1965	6	2
3	3	6.43	2.14	1966	1	8	1966	1	10
4	3	7.85	2.62	1966	1	30	1966	2	1
5	4	8.32	2.08	1966	10	1	1966	10	4
6	5	12.39	2.48	1973	2	22	1973	2	26
7	16	40.21	2.51	1974	1	7	1974	1	22
8	4	9.59	2.40	1978	3	10	1978	3	13
9	3	6.38	2.13	1978	7	13	1978	7	15
10	3	9.01	3.00	1979	1	19	1979	1	21
11	3	7.14	2.38	1981	5	19	1981	5	21
12	3	7.67	2.56	1981	7	7	1981	7	9
13	3	7.35	2.45	1987	1	9	1987	1	11
14	11	29.01	2.64	1988	11	17	1988	11	27
15	3	6.89	2.30	1992	1	27	1992	1	29
16	12	26.19	2.18	1992	8	3	1992	8	14
17	3	7.89	2.63	1993	1	4	1993	1	6
18	3	7.68	2.56	1997	2	5	1997	2	7
19	4	9.00	2.25	1999	2	12	1999	2	15
20	4	8.48	2.12	2000	4	1	2000	4	4
21	3	6.36	2.12	2001	5	14	2001	5	16

22	9	20.76	2.31	2001	5	18	2001	5	26
23	3	7.69	2.56	2001	12	13	2001	12	15
24	4	8.62	2.16	2002	6	12	2002	6	15
25	3	7.53	2.51	2004	12	14	2004	12	16
26	4	9.06	2.26	2005	7	5	2005	7	8
27	3	6.61	2.20	2005	8	12	2005	8	14
28	3	6.65	2.22	2005	9	19	2005	9	21
29	6	14.63	2.44	2006	8	30	2006	9	4
30	4	9.57	2.39	2006	9	25	2006	9	28
31	3	6.54	2.18	2007	10	5	2007	10	7
32	3	6.91	2.30	2008	9	21	2008	9	23
33	3	7.14	2.38	2008	12	1	2008	12	3
34	17	45.81	2.69	2008	12	9	2008	12	25
35	3	6.69	2.23	2009	8	26	2009	8	28
36	4	9.10	2.28	2009	9	5	2009	9	8
37	3	6.60	2.20	2011	8	16	2011	8	18
38	3	7.05	2.35	2011	8	20	2011	8	22
39	10	23.18	2.32	2011	8	29	2011	9	7
40	4	9.42	2.35	2013	3	6	2013	3	9
41	22	58.22	2.65	2013	7	28	2013	8	18
42	5	12.76	2.55	2013	10	10	2013	10	14
43	5	10.93	2.19	2014	1	23	2014	1	27
44	6	14.35	2.39	2014	1	29	2014	2	3
45	5	10.90	2.18	2015	1	21	2015	1	25
46	8	18.41	2.30	2015	10	19	2015	10	26
47	3	6.53	2.18	2016	9	24	2016	9	26
48	3	6.27	2.09	2017	11	8	2017	11	10
49	9	20.67	2.30	2019	8	20	2019	8	28
50	7	17.86	2.55	2019	9	29	2019	10	5
51	3	6.85	2.28	2019	10	9	2019	10	11
52	5	13.13	2.63	2021	10	1	2021	10	5
53	6	15.98	2.66	2022	7	12	2022	7	17
54	41	112.71	2.75	2022	8	11	2022	9	20
55	6	15.37	2.56	2022	9	29	2022	10	4
56	15	35.58	2.37	2022	10	14	2022	10	28
57	5	10.98	2.20	2022	10	30	2022	11	3
58	4	10.63	2.66	2022	11	9	2022	11	12
59	3	6.45	2.15	2023	9	9	2023	9	11
60	4	9.05	2.26	2023	12	6	2023	12	9